Chinese Journal of Natural Medicines

Ziyuglycoside II suppressed the progression of osteosarcoma by coordinating estrogen-related receptor gamma and p53 signaling pathway

Hang Du, Dongjin Wu, Tianyu Zhang, Ying Zhong, Kaiyi Wu, Xin Guo, Lisong Sheng, Nana Huang, Chunzheng Gao, Rong Sun

Citation: Hang Du, Dongjin Wu, Tianyu Zhang, Ying Zhong, Kaiyi Wu, Xin Guo, Lisong Sheng, Nana Huang, Chunzheng Gao, Rong Sun, Ziyuglycoside II suppressed the progression of osteosarcoma by coordinating estrogen-related receptor gamma and p53 signaling pathway, Chinese Journal of Natural Medicines, 2025, 23(3), 354-367. doi: 10.1016/S1875-5364(25)60847-8.

View online: https://doi.org/10.1016/S1875-5364(25)60847-8

Chinese Journal of Natural Medicines 23 (2025) 354-367

Contents lists available at ScienceDirect

Chinese Journal of Natural Medicines

journal homepage: www.cjnmcpu.com/

Original article

Ziyuglycoside II suppressed the progression of osteosarcoma by coordinating estrogen-related receptor gamma and p53 signaling pathway

Hang Du[a], Dongjin Wu[a], Tianyu Zhang[a,c], Ying Zhong[a], Kaiyi Wu[a,d], Xin Guo[a,d], Lisong Sheng[b], Nana Huang[a,c], Chunzheng Gao[a,*], Rong Sun[a,b,*]

[a] *The Second Hospital of Shandong University, Jinan 250033, China*
[b] *Advanced Medical Research Institute, Shandong University, Jinan 250012, China*
[c] *Academy of Traditional Chinese Medicine, Shandong University of Traditional Chinese medicine Jinan 250355, China*
[d] *School of Pharmacy, Tianjin University of Traditional Chinese medicine, Tianjin 301617, China*

ARTICLE INFO

Article history:
Received 26 December 2023
Revised 19 April 2024
Accepted 28 April 2024
Available online 20 March 2025

Keywords:
Ziyuglycoside II
Osteosarcoma
Cell cycle arrest
p53
Estrogen-related receptor gamma

ABSTRACT

Osteosarcoma (OS) is the most prevalent primary malignant bone tumor affecting children and adolescents. Despite ongoing research efforts, the 5-year survival rate has remained stagnant for many years, highlighting the critical need for novel drug development to enhance current treatment protocols. Ziyuglycoside II (ZYG II), a triterpenoid saponin extracted from S. officinalis, has recently demonstrated antitumor properties. This study evaluates the antitumor effect of ZYG II on osteosarcoma and elucidates its mechanism of action through the co-regulation of p53 and estrogen-related receptor gamma (ESRRG), which inhibits disease progression. The research employs *in vitro* experiments using multiple established osteosarcoma cell lines, as well as *in vivo* studies utilizing a nude mouse model of orthotopic xenograft osteosarcoma. Additionally, ESRRG shRNA was used to construct stable ESRRG-reducing OS cell lines to investigate the molecular mechanism by which ZYG II exerts its anti-osteosarcoma effects through the co-regulation of ESRRG and p53. Results indicate that ZYG II administration led to decreased OS cell viability and reduced tumor volumes. Furthermore, cell cycles were arrested at the G_0/G_1 phase, while the proportion of apoptotic cells increased. Expression of p53, ESRRG, p21, Bax, Cleaved Caspase-9, and Cleaved Caspase-3 proteins increased, while expression of CDK4, Cyclin D1, and Bcl-2 proteins decreased. Multiple ZYG II and ESRRG docking patterns were simulated through molecular docking. Comparing the pharmacodynamic response of ZYG II to OS cell lines with reduced ESRRG and normal expression demonstrated that ZYG II inhibits osteosarcoma progression, induces cell cycle arrest, and promotes cell apoptosis through the coordination of p53 and ESRRG. In conclusion, ZYG II inhibits osteosarcoma progression, leads to cell cycle arrest, and promotes cell apoptosis through synergistic regulation of p53 and ESRRG.

1. Introduction

Osteosarcoma (OS) is the most prevalent primary malignant bone tumor in children and adolescents (incidence: 4.3/1 000 000/year), and the second leading cause of cancer-related mortality in this demographic [1,2]. OS originates from bone mesenchymal cells, primarily emerging in the metaphysis of long bones, and has been substantiated to have a close association with skeletal growth rate [2,3]. Currently, the 5-year survival rate for localized osteosarcoma is approximately 60%–75%, while for metastatic disease, it is only 20%–40% [2]. Over the past few decades, the incidence and prevalence of osteosarcoma in children and adolescents have steadily increased [4]. The most commonly utilized chemotherapeutic drugs with known high efficacy are adriamycin, high-dose methotrexate, cisplatin, and ifosfamide. However, these are associated with side effects, including liver and kidney function impairment, bone marrow suppression, neurotoxicity, and gastrointestinal reactions, among others [5]. Despite extensive study and research, minimal improvements have been made in the treatment of osteosarcoma since the mid-1990s, largely due to the scarcity of milestone advancements in more effective novel agents [4]. Given the limitations of conventional treatment regimens, there is an urgent need to develop innovative therapeutic strategies aimed at improving the overall survival of patients with osteosarcoma [6].

The sequential mechanisms underlying osteosarcomagenesis are not fully elucidated. The most probable sequence of events leading to osteosarcoma development involves the loss of TP53 and RB1 as initial occurrences, with TP53 loss likely initiating genomic instability [7]. The subsequent depletion of p53 in osteosarcoma results in the dysregulation of numerous oncogenes, including the amplification of c-Myc and the depletion of PTEN. Among

* Corresponding author.
E-mail addresses: gaochunzheng1964@sina.com (C. Gao); sunrong@sdu.edu.cn (R. Sun)

https://doi.org/10.1016/S1875-5364(25)60847-8

these, the most significantly affected genes are related to cell cycle and apoptosis [8-10]. Additionally, the p53 protein encoded by TP53 can modulate the expression of proteins such as p16, p21, p27, CDK4, and Rb, leading to cell cycle arrest [11].

Conversely, p53-mediated transcriptional activation induces Noxa, Puma, Bim, and Bax, resulting in changes to mitochondrial membrane permeability, cytochrome c release, and subsequent activation of Caspase proteins, ultimately leading cells through the apoptotic process [12]. These dysregulated mechanisms may offer potential therapeutic targets; however, our understanding of the molecular mechanisms underlying osteosarcoma cell proliferation remains incomplete.

Research efforts are currently focused on exploring alternative approaches to osteosarcoma treatment beyond systemic chemotherapy, with a significant emphasis on novel therapeutic agents derived from Chinese herbal extracts [6, 9]. *Sanguisorba officinalis* L. (*S. officinalis*), a member of the Rosaceae family, has been traditionally utilized in Chinese medicine. It is recognized for its diverse beneficial properties, including hemostatic, detoxifying, anti-inflammatory, analgesic, antibacterial, anti-tumor, and neuroprotective effects [13, 14]. Ziyuglycoside II (ZYG II), a triterpenoid saponin compound extracted from *S. officinalis*, has demonstrated suppressive properties in various human cancer types [15, 16]. Research indicates that ZYG II inhibits the proliferation of BGC-823 human gastric carcinoma cells by inducing mitochondrial apoptosis, specifically through the regulation of Bax/Bcl-2 expression and activation of the caspase-3 pathway [17]. Furthermore, ZYG II exhibits a dual mechanism in human colon cancer cells, inducing apoptosis through both p53-induced caspase-dependent and caspase-independent pathways. This process is characterized by decreased expression of BCL-2, mitochondrial targeting, altered production of reactive oxygen species (ROS), and translocation of apoptosis inducing factor (AIF) to the nuclei [18].

Two recent studies concur that among various digestive system tumors, hepatoma carcinoma cells demonstrate increased sensitivity to the anti-proliferative effects of ZYG II. This compound inhibits EGFR phosphorylation, thereby modulating downstream signaling pathways such as NF-κB or ERKs, inducing G_0/G_1 phase arrest or apoptosis, and ultimately reducing the activity of liver cancer cells [16, 19]. Beyond digestive system tumors, ZYG II also suppresses breast cancer development through its modulation of the p53/p21, ROS/JNK, and Src/EGFR-dependent ITGB4/FAK signaling pathways. This leads to ROS accumulation, cell cycle arrest, apoptosis, epithelial-mesenchymal transition, and resistance to anoikis [20-22]. Furthermore, ZYG II inhibited angiogenesis, enhanced hematopoietic function, and counteracted leukopenia, all of which are critical factors in inhibiting tumor development and improving tumor prognosis [23-25].

The orphan receptor estrogen-related receptor gamma (ESRRG) is a member of the estrogen-related receptor (ERR) family, which belongs to group III of the nuclear receptor superfamily [26]. ESRRG plays a significant role in the progression of various human malignancies. It induces p21 and p27 expression through direct transactivation of their gene promoters, thereby inhibiting the proliferation of prostate and liver cancer [27, 28]. Notably, the selective ESRRG agonist, DY131, enhances ESRRG-induced growth inhibition in a dose-dependent manner, suggesting a potential pharmacological approach for prostate cancer treatment targeting ESRRG [28]. Furthermore, gene expression analysis indicates that ESRRG inhibits Wnt signaling by blocking the adhesion of TCF4/LEF1 to the CCND1 promoter, which initiates Cyclin D1 protein transcription, thereby suppressing the proliferation and oncogenesis of gastric cancer cells [29]. Additionally, ESRRG is implicated in the pathogenesis of retinal neuroblastoma and various female cancers, including breast and endometrial cancers [30-32]. Existing research suggests that ESRRG and ZYG II exhibit similar functional characteristics in suppressing different tumor types, targeting both comparable tumor types and centrally regulating cell cycle and apoptosis induction in their anti-tumor mechanisms. Consequently, ZYG II's antitumor effects may be associated with its relationship to ESRRG.

ESRRG plays a significant role in bone metabolism regulation. During bone formation, ESRRG regulates osteopontin promoters based on cellular environmental homogeneity and differences [33]. A study using a global knockout mouse model for ESRRG revealed that ESRRG deletion minimally affected congenital bone development. However, in the acquired bone formation process, ESRRG promotes osteoblast differentiation and matrix mineralization in 8-week-old male mice by regulating alkaline phosphatase, bone sialoprotein, and *RUNX2* genes [34]. In bone resorption, ESRRG *via* attenuation of RANKL-mediated expression of c-Fos and nuclear factor of activated T-cells cytoplasmic 1, interferes with osteoclastogenesis and accelerates osteoclast apoptosis through caspase-3 activation [35]. ESRRG's influence on various tumors and bone metabolism suggests a potential unique role in osteosarcoma. Consequently, bone tumors may provide a promising platform for further investigation into how ZYG II regulates ESRRG-related mechanisms during tumor suppression.

This study conducted *in vivo* and *in vitro* experiments to investigate the efficacy and elucidate the pharmacological and molecular mechanisms of ZYG II in inducing cell cycle arrest and apoptosis in osteosarcoma. Furthermore, the research employs short-hairpin RNA (shRNA) to suppress ESRRG (ESRRG shRNA) and an ESRRG inverse agonist, GSK5182, in p53-positive MG-63 cells and p53-negative SaOS-2 cells to examine the relationship between ESRRG and p53.

2. Materials and Methods

2.1. Regents and antibodies

ZYG II (purity > 99%, *Mr*: 604.8) was obtained from the National Institute for the Control of Pharmaceutical and Biological Products (Beijing, China). Dulbecco's modified Eagle's medium (DMEM) and dimethyl sulfoxide (DMSO) were procured from Sigma Chemical (St. Louis, MO, USA). Fetal bovine serum (FBS), penicillin G, and streptomycin solution were acquired from GIBCO BRL (Gaithersburg, MD, USA). The Annexin V-FITC and propidium iodide (PI) double staining kit was purchased from BD Biosciences (CA, USA). Enhanced Cell Counting Kit-8 (CCK-8), EdU Cell Proliferation Kit with Alexa Fluor 555, and Stripping Buffer were obtained from Beyotime Institute of Biotechnology (Hangzhou, China). Hematoxylin-eosin (H&E) staining was performed through Service Biotechnology (Wuhan, China). GSK5182 and Cycloheximide (CHX) were acquired from MedChemExpress (Monmouth, NJ, USA). The primary antibody to ESRRG (T58712) was obtained from Abmart Pharmaceutical Technology (Shanghai, China). The primary antibodies to p53 (#2527), p21 (#2947), CDK4 (#12790), cyclin D1 (#55506), Bax (#5023), Bcl-2 (#4223), cleaved caspase-9 (#9505), cleaved caspase-3 (#9664), and β-actin (#4970) were purchased from Cell Signaling Technology (Danvers, USA).

2.2. Cell lines and culture

Osteosarcoma cell lines MG-63, SaOS-2, U2-OS, and SJSA-1 were obtained from the Cell Bank of the Chinese Academy of Sciences, China. Each osteosarcoma cell line was cultured in appropriate media: DMEM, McCoy's 5A, or RPMI 1640, supplemented with 10% fetal bovine serum and 1% Penicillin-Streptomycin solution. The cells were maintained at 37 °C in a humidified incubator with a 5% CO_2 atmosphere.

2.3. Lentiviral infection

The ESRRG knockdown procedures were conducted in accordance with the manufacturer's instructions. ESRRG shRNA lentiviruses were obtained from GeneChem Inc. (Shanghai, China). MG-63 and SaOS-2 cells (4×10^5) were infected with shRNA lentiviruses and control adenovirus (MOI = 50) and incubated at 37 °C for 48 h. Puromycin (final concentration: 2 $\mu g \cdot mL^{-1}$) was utilized to select stable MG-63 and SaOS-2 cells with down-regulated ESRRG for two weeks. The following target sequences were employed in the present experiments: ESRRG shRNA-1: GCTGAACCGGAGAAGATCTAT; ESRRG shRNA-2: GGACGAAGACCAGTCCAAATT; ESRRG shRNA-3: GCTATCCTGCAGCTGGTAAAG.

2.4. CCK-8 assay

Osteosarcoma cell lines MG-63, SaOS-2, U2-OS, and SJSA-1 (1×10^4 cells per well) in the logarithmic growth phase were cultured in 96-well plates for 24 hours. Subsequently, the medium was replaced with 0.2 mL of drug-containing medium. The experimental groups consisted of ZYG II at various concentrations (2.5, 5, 10, 15, 20, 25, 30, 40, 50 $\mu mol \cdot L^{-1}$) applied to MG-63, SaOS-2, U2-OS, and SJSA-1 cells. The control group (with cells) received an equivalent amount of drug carrier solvent (DMSO content < 0.3%), while the blank group (without cells) received only the same volume of medium. Following drug administration, cell viability was assessed using the CCK-8 kit. After adding 10 μL of CCK-8 stock solution to each well, the plates were incubated at 37 °C for 2 hours. Absorbance was then measured at 450 nm using a Microplate reader (Bio-Rad, CA, USA). IC_{50} values were calculated through nonlinear regression analysis of survival curves using SPSS software version 13.0. Each concentration was tested in six replicates, and the experiment was performed in triplicate. Results are presented as mean ± SEM.

2.5. EdU assay

Osteosarcoma cells were cultured in 96-well plates at a density of 1×10^4 cells per well and incubated for 24 hours. Subsequently, ZYG II was added at concentrations of 0, 5, 10, 15, or 20 $\mu mol \cdot L^{-1}$ and incubated for an additional 24 hours. 5-Ethynyl-2'-deoxyuridine (EdU) reagent, diluted 1∶1000, was then applied to the cells for 4 hours. Following this, the cells were fixed with 4% paraformaldehyde and stained with fluorescent dyes and Hoechst. Finally, Image J software (version 1.8.0) was utilized to quantify the number of EdU-positive cells.

2.6. Flow cytometry analysis of cell cycle analysis

The cells were harvested after 24 hours of treatment in serum-free medium with corresponding concentrations of ZYG II (5, 10, 15, or 20 $\mu mol \cdot L^{-1}$). To fix the cells, cold 75% ethanol was utilized. Following 12 hours of cold storage, the cells were washed with cold PBS. PI staining was then applied according to the manufacturer's instructions, and the sample was incubated in darkness at 37 °C for 30 minutes. A flow cytometer (CytoFLEX, Beckman Coulter) was employed for online detection and analysis.

2.7. Flow cytometry analysis of apoptosis analysis

Cells underwent treatment with corresponding concentrations of ZYG II for 24 hours, followed by digestion and collection using pancreatic enzymes. The cells were then washed twice with ice-cold PBS and re-suspended. Subsequently, the cells were incubated in 100 μL of 1× binding buffer containing 5 μL of Annexin V-FITC stock and 5 μL of PI for 15 minutes in darkness at room temperature. Following staining, 400 μL of binding buffer was added to each tube, and the samples were analyzed using flow cytometry.

2.8. Animal study

Twenty-four male BALB/c nude mice, aged six weeks, were obtained from Beijing Vital Laboratory Animal Technology [Beijing, China, Certificate No. SCXK (Jing) 2019-0010]. The mice were maintained under standard conditions: temperature (22 ± 2 °C), humidity (55% ± 10%), and light (12 h light/dark cycle) in specific pathogen-free conditions at the Laboratory Animal Center of Shandong University (Jinan, China). The animal procedures were approved by the Ethics Committee of the Second Hospital of Shandong University [Ethics Committee Approval No: KYLL-2021(KJ)P-0362].

The orthotopic xenograft model of osteosarcoma was established using surgical orthotopic implantation [36]. Nude mice were anesthetized prior to the procedure for creating the orthotopic xenograft model of an OS tumor. An approximately 10 mm incision was made on the right thigh. The vastus lateralis and biceps femoris muscles were separated, and the patellofemoral ligament was incised without compromising the knee joint. Subsequently, the lateral condyle of the femur was removed, and a tumor fragment (3–4 mm^3) of MG-63, previously harvested from a subcutaneously-implanted tumor that had grown to more than 10 mm in diameter, was implanted into the created space. Six-zero nylon sutures were utilized to close the muscle and wound.

One week following the surgical procedure, tumor dimensions were assessed, and the nude mice were divided into four groups: the model group (vehicle, Mod), ZYG II low (10 $mg \cdot kg^{-1}$, Low), medium (20 $mg \cdot kg^{-1}$, Mid), and high (40 $mg \cdot kg^{-1}$, High) dosage groups. The vehicle solution consisted of 10% DMSO, 40% PEG300, 5% Tween 80, and 45% saline.

For 28 days, nude mice received daily intragastric doses, with body weight and tumor size measurements taken twice weekly. The Relative Tumor Volume (RTV) and Relative Tumor Proliferation Rate [$T/C(\%)$] were calculated to compare tumor sizes and anti-tumor efficacy across groups for both bone and soft tissue tumors. Tumor volume was measured using a caliper and calculated using the formula: Tumor Volume (*Tumor Volume* (*TV*)) (mm^3) = $L \times W^2/2$, where L represents length and W represents width. The RTV for each group was determined using the equation TV^n / TV^0, with TV^n representing the tumor volume on a specific day, and TV^0 as the tumor volume on day 0. The T/C% was calculated using the formula TRTV/CRTV × 100%, where TRTV represents the RTV for the treatment group and CRTV refers to the RTV for the control group. The mean ± SEM were calculated for all groups, and statistical significance was determined using two-way ANOVA.

2.9. H&E staining

Xenograft tumor and liver tissues from various experimental groups were fixed in 4% paraformaldehyde for two days, sectioned to 4 μm thickness, and embedded in paraffin. Subsequently, the sections underwent deparaffinization with xylene and rehydration using a graded ethanol series. H&E staining was then performed following established protocols.

2.10. Molecular docking simulation

The molecular structure of ZYG II was acquired from the PubChem Compound Database. The 3D coordinates of ESRRG ligand-binding domain in the constitutively active conformation (PDB ID: 1KV6) were obtained from PDB. The target protein ESRRG was separated from the original ligand steroid receptor coactivator-1 (SRC-1) using PyMOL (version 2.3.0). The 3D structure files of ESRRG, ZYG II, and SRC-1 were converted into PDBQT format, with all water molecules removed and polar hydrogens added. Initially, molecular docking of ESRRG with the

primary ligand SRC-1 was performed. Gridboxes were centered to encompass the structural domain of each protein and accommodate free molecular motion. The binding pocket was defined as a 30 Å × 30 Å × 30 Å cuboid, with a grid spacing of 0.05nm. The SRC-1 site was utilized as the active pocket of ESRRG protein for molecular docking between ESRRG and ZYG II. The highest-scoring pose (ranked by affinity score: kcal·mol^{-1}) was chosen for subsequent analysis and visualization. Molecular docking studies were conducted using Autodock Vina 1.2.2 for model visualization.

2.11. Western blotting analysis

Total protein from OS cells or tissue was extracted using RIPA Lysis Buffer (strong) containing protease and phosphatase inhibitors on ice. Protein concentrations were determined using the BCA method and diluted to 1 μg·μL^{-1}. The protein extracts were separated on SDS-polyacrylamide gels and subsequently transferred onto polyvinylidene difluoride (PVDF) membranes. After blocking with 5% skim milk powder solution for 60 min at room temperature, the PVDF membranes were cut according to the molecular weight of the target protein. The membranes were then incubated overnight at 4 °C with primary antibodies against p53, p21, CDK4, Cyclin D1, Bax, Bcl-2, Cleaved Caspase-9, Cleaved Caspase-3, ESRRG, and *β*-actin. Following incubation with secondary antibodies for 2 h at room temperature, the signals on PVDF membranes were enhanced using an ECL assay kit, and the blots were visualized using a luminescent image analyzer (Tanon 5200 Multi, Shanghai, China). The former band was stripped with Stripping buffer and incubated with other antibodies.

2.12. Immunohistochemistry

The Immunohistochemistry (IHC) staining protocol for osteosarcoma sections commenced with incubation in an anti-ESRRG antibody solution (1∶100). Antigen retrieval was performed using a citric acid buffer high-pressure heating method. Subsequently, the sections underwent a 10-minute immersion in pure hydrogen peroxide at room temperature, followed by two 5-minute washes with TBS. The slices were then subjected to a 30-minute goat serum incubation at room temperature, after which they were refrigerated at 4 °C to facilitate primary antibody attachment. The following day, the secondary antibody was applied to the slices for 30 minutes at room temperature. The process concluded with DAB application for color development and hematoxylin staining of the nuclei. Following IHC staining, the Integral optical density (IOD) was quantified using Image-ProPlus 6.0 software.

2.13. Immunofluorescence

Cells were initially fixed with ice-cold 2% paraformaldehyde, followed by permeabilization with 0.2% Triton X-100 (Tx100). For fluorescence labeling preparation, post-fixation cells underwent brief extraction for 30 seconds at 37 °C using a PEM buffer composed of 100 mmol·L^{-1} PIPES (adjusted to pH 6.8), 1 mmol·L^{-1} EGTA, and 1 mmol·L^{-1} $MgCl_2$, supplemented with 0.5% T × 100. The cells were subsequently post-fixed with ice-cold methanol. The fixed cells were then incubated for 1 h in a 1% bovine serum albumin (BSA) solution to block non-specific binding sites. Following this, they were exposed to primary antibodies for 1 hour, facilitating antigen binding within the cells. A 45-minute incubation with fluorophore-conjugated secondary antibodies ensued. Finally, the immunostained cells were mounted onto slides using VECTASHIELD mounting medium from Vector Laboratories, Burlingame, CA. All images were captured at the same magnification, spanning a length of 200 μm.

2.14. Statistical analysis

Statistical analyses were performed using the SPSS 16.0 software package (Chicago, IL, USA). All studies were conducted at least three times unless otherwise specified. Results are presented as mean ± SEM. Statistical differences between two populations were determined using a two-tailed Student's *t* test. A *P* value of $P< 0.05$ was considered statistically significant.

3. Results

3.1. ZYG II has anti-proliferative activity in OS cells

The effectiveness of ZYG II on OS cell activity and proliferation was evaluated using both CCK-8 and EdU assays. *In vitro*, ZYG II demonstrated a concentration-dependent reduction in OS cell viability. Through nonlinear regression analysis, the *in vitro* half maximal inhibitory concentration (IC_{50}) of ZYG II was determined for MG-63, SaOS-2, SASJ-1, and U2-OS cells, yielding values of 15.62, 17.80, 19.90, and 20.55 μmol·L^{-1}, respectively (Figs. 1A and S1A). The negative control treatment exhibited no effect on cell viability.

Utilizing red fluorescence for EdU and blue fluorescence for Hoechst 33342, the study determined the proportion of EdU-positive and Hoechst 33342-positive cells in the MG-63 and SaOS-2 cell lines to be (66.75 ± 2.26)% and (68.01 ± 2.33)% respectively in the control group (Figs.1 B and 1C). Following the application of ZYG II at concentrations of 5, 10, 15, and 20 μmol·L^{-1} for 24 h, cell proliferation rates in MG-63, SaOS-2, SASJ-1, and U2-OS cells exhibited significant decreases, with the exception of the 5 μmol·L^{-1} concentration (Figs. 1 & S1).

3.2. ZYG II induces G_0/G_1 cell cycle arrest and apoptosis in OS cells

Flow cytometry was employed to analyze the cell cycle progression and apoptosis of MG-63 and SaOS-2 cells following 24 h of ZYG II treatment. Cell cycle analysis revealed an increase in cell counts within the G_0/G_1 phase and a decrease in the S phase after 24 h of ZYG II treatment in both MG-63 and SaOS-2 cells (Figs. 2A and 2C). Apoptosis analysis demonstrated a reduction in the proportion of Annexin V−/PI− cells, an increase in Annexin V+/PI− cells, and no significant changes in Annexin V+/PI+ cells (Figs. 2 B and 2D). The cell cycle and apoptosis data for U2-OS and SJSA-1 cells are presented in Supplementary Fig. 2. These findings indicate that ZYG II effectively arrested OS cells at the G_0/G_1 phase while inducing apoptosis rather than necrosis.

3.3. ZYG II inhibits OS progression in an orthotopic xenograft model

The administration of ZYG II inhibited tumor growth, resulting in a slower increase in RTV for the middle and high dose groups (Figs. 3 B and 3C). However, no significant difference was observed between the low-dose group and the control group. The T/C (%) values for the low, middle, and high dose ZYG II groups were (102.9 ± 24.5)%, (57.3 ± 18.6)%, and (20.6 ± 4.7)%, respectively.

(Fig. 3D) revealed notable morphological alterations in the tumor sections. The nuclei exhibited hyperchromasia, pyknosis, fragmentation, and dissolution. Additionally, pink-staining amorphous material was observed, indicative of cell necrosis, as highlighted by the yellow arrows.

Histological examination of liver tissue using hematoxylin and eosin (HE) staining revealed no significant pathological differences between the model group and the ZYG II administration

group. Furthermore, no pathological manifestations, such as steatosis or inflammation, were observed in the liver tissues of any ZYG II dosage group. Serological analysis demonstrated that ZYG II administration did not elevate serum aspartate aminotransferase (AST), alanine aminotransferase (ALT), or other liver injury markers (Fig. S3).

3.4. ZYGII upregulated ESRRG expression and activated p53-mediated cycle and apoptosis-related signaling pathways

The impact of ZYG II on OS p53, ESRRG, cell cycle, and apoptosis-related protein expressions was examined through *in vitro* efficacy validation, as well as cell cycle and apoptosis detection

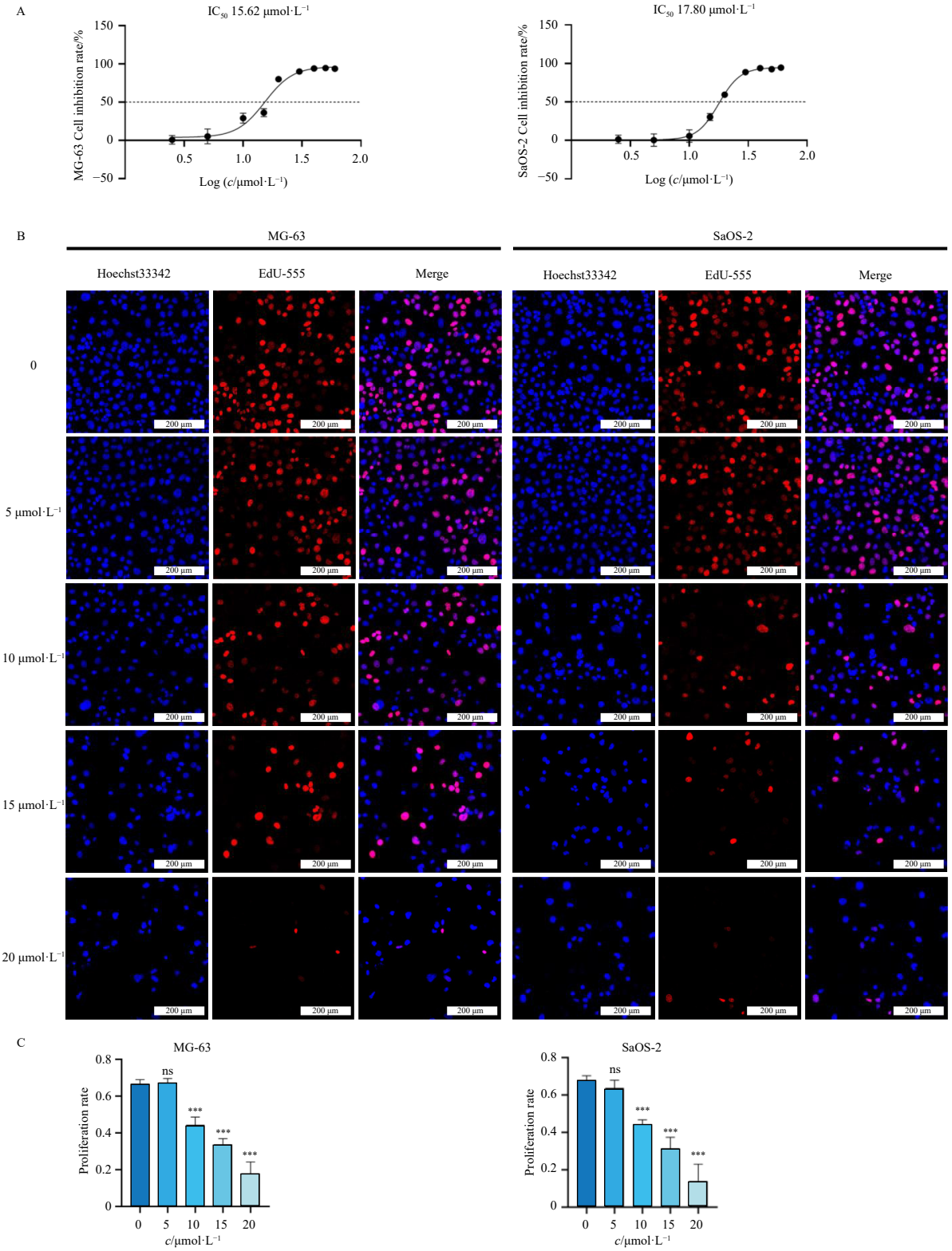

Fig. 1 ZYG Ⅱ inhibited the activity and proliferation of OS cells *in vitro*. (A) The cell viability and nonlinear regression results of IC_{50} of MG-63 and SaOS-2 cells were examined by CCK-8 assay after the treatment with various concentrations of ZYG II for 24 h (n = 6). (B) MG-63 and SaOS-2 cell proliferation rates were detected by EdU staining after the treatment with 0, 5, 10, 15 and 20 μmol·L^{-1} of ZYG II for 24 h. Red staining indicates proliferation (EdU +), while blue staining indicates . Scale bar: 200 μm. (C) EdU incorporation was calculated as EdU+ cells/total cells, quantified by ImageJ (n = 3). All data are presented as mean ± SEM from three independent experiments ($^{*}P$ < 0.05, $^{**}P$ < 0.01 and $^{***}P$ < 0.001 *vs* Con).

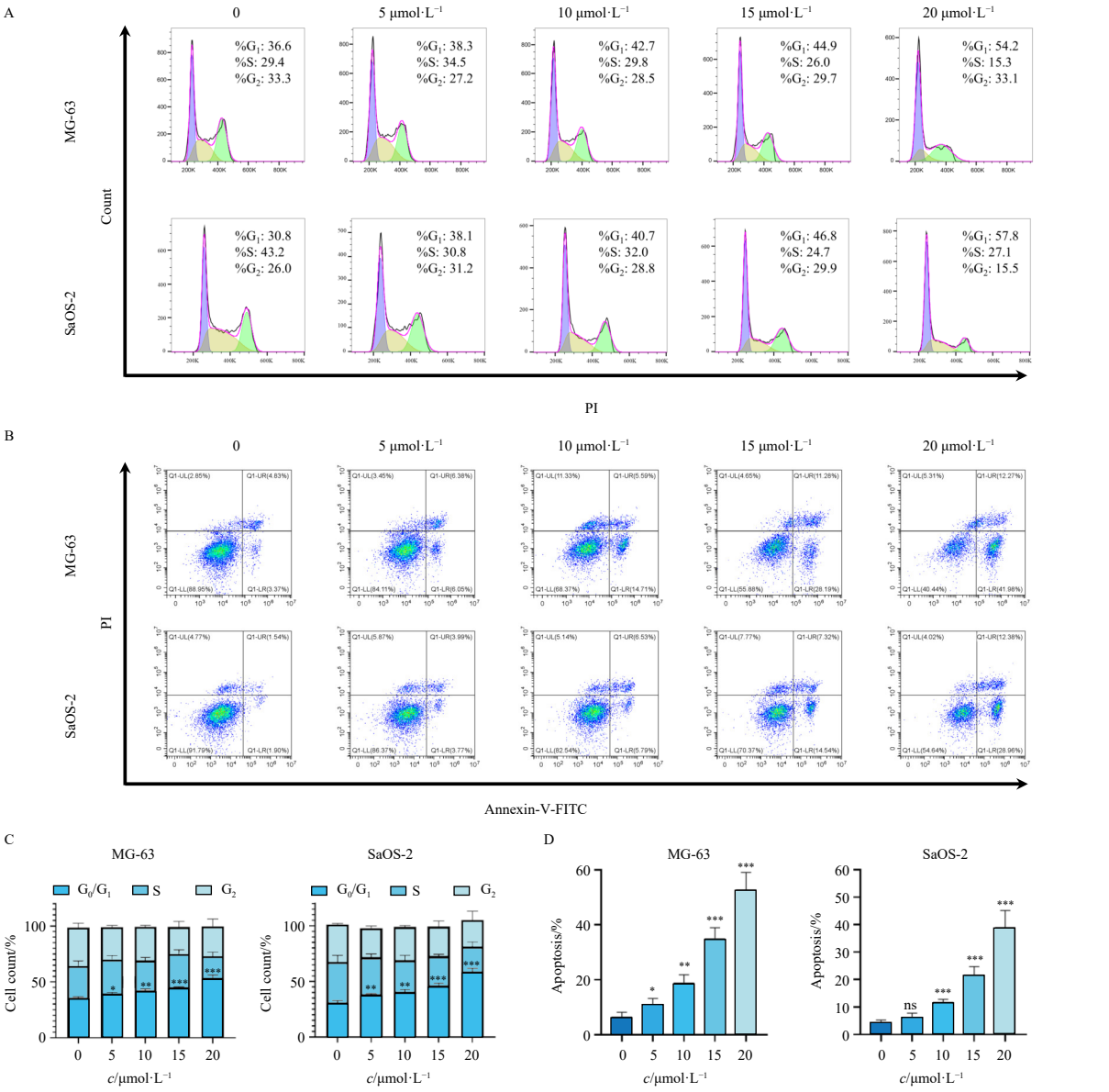

Fig. 2 ZYG Ⅱ regulated the MG-63 and SaOS-2 cell cycle and apoptosis. (A, C) Cell cycle distribution of MG-63 cells and SaOS-2 cells with the treatment of ZYG Ⅱ for 24 h. (B, D) Pro-apoptotic capacities of ZYG Ⅱ against MG-63 cells and SaOS-2 cells after co-incubation for 24 h. Live cells were represented by Annexin V−/PI−, apoptosis cells were represented by Annexin V+/PI−, Late apoptotic and necrotic cells were represented by Annexin V+/PI+, and schistocytes generated by mechanical damage were represented by PI+/Annexin+. All data are expressed as mean ± SEM (n = 3). $^{*}P < 0.05$, $^{**}P < 0.01$ and $^{***}P < 0.001$ *vs* Con.

assays. Apart from the absence of p53 expression in SaOS-2 cells, ZYG II treatment resulted in increased levels of p53, ESRRG, p21, Bax, Cleaved Caspase-9, and Cleaved Caspase-3 in osteosarcoma cells. Conversely, the expressions of CDK4, Cyclin D1, and Bcl-2 decreased in a dose-dependent manner following ZYG II administration (Figs. 4 A and 4B).

To further elucidate the regulatory influence of ZYG II on ESRRG, we employed green fluorescent tagging to monitor ESRRG expression. Untreated osteosarcoma cells exhibited low fluorescence intensity, suggesting limited ESRRG expression. After 24 hours of exposure to 15 μmol·L^{-1} ZYG II, a significant increase in green fluorescence was observed within the cells, indicating elevated ESRRG expression (Fig. 4D).

3.5. ZYG II mitigated the negative effects of protein synthesis pathways on ESRRG protein expression

To elucidate the mechanism by which ZYGII regulates ESRRG protein expression levels, OS cells were treated with CHX at 10 μmol·L^{-1} for 24 h. Western blot analysis revealed a decrease in ESRRG protein expression in CHX-treated cells compared to untreated controls. Notably, when ZYG II and CHX were administered simultaneously, ESRRG protein expression was more pronounced than in cells treated with CHX alone. This suggests that ZYG II can maintain ESRRG protein expression independently of the protein synthesis pathway. Moreover, ZYG II appeared to mitigate the inhibitory effects of protein synthesis inhibition on ESRRG protein expression (Fig. 4E).

3.6. ZYG II regulates OS protein expression in an orthotopic xenograft model

Following the extraction of tumor tissues, a portion was utilized for protein extraction and subsequent Western blot (WB) analysis. The results demonstrated that in the middle and high dose groups of ZYG II, the protein expression levels of p53, ESRRG, p21, Bax, Cleaved Caspase-9, and Cleaved Caspase-3 were upregulated, while CDK4, Cyclin D1, and Bcl-2 protein expression levels were downregulated (Fig. 5A). No significant differences in protein expression were observed between the low dose group of ZYG II and the control group.

IHC was also employed to detect ESRRG protein expression

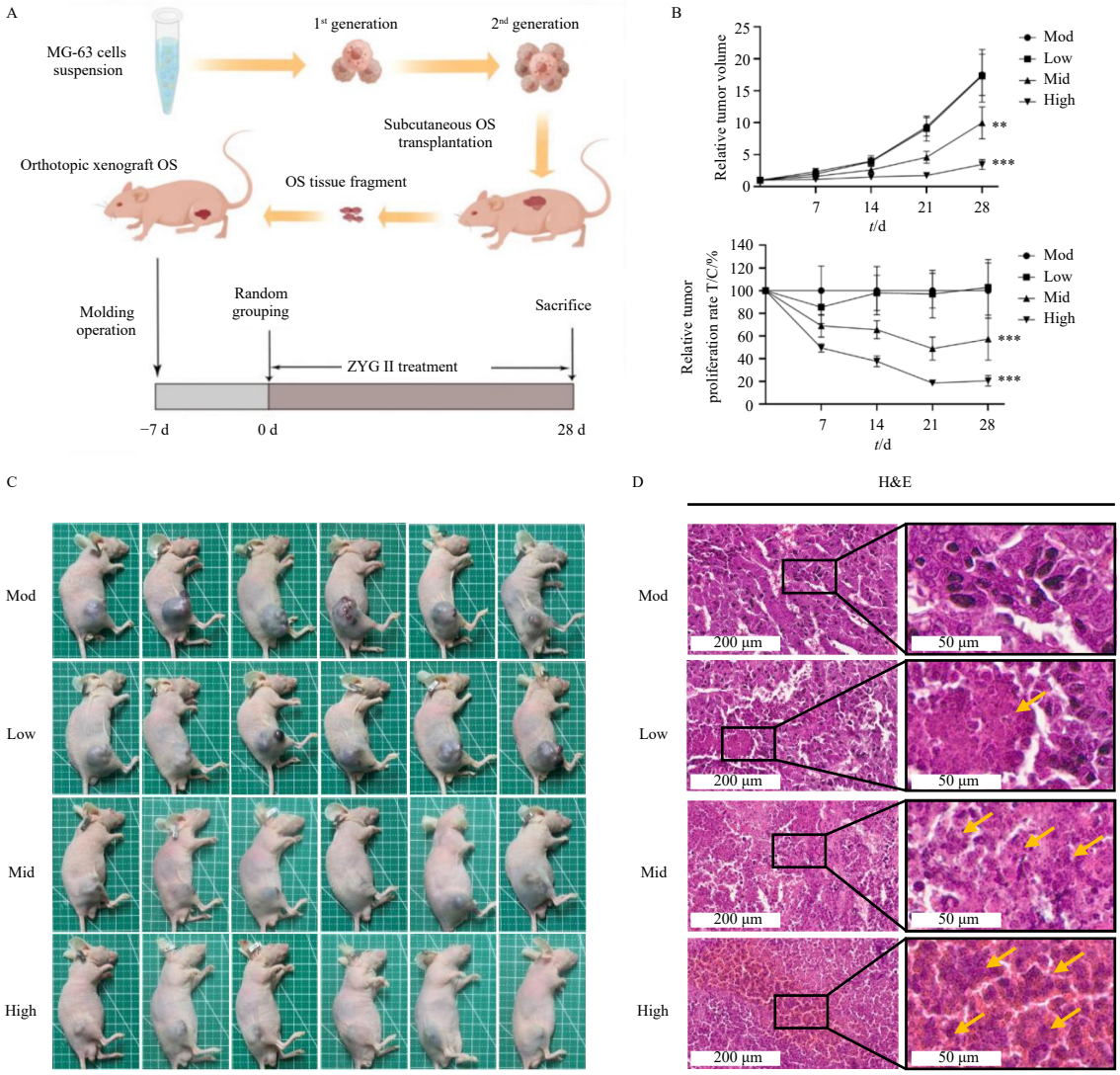

Fig. 3 ZYG Ⅱ inhibited OS *in vivo*. (A) Animal experimental flowchart. (B) Changes in relative tumor volume and relative tumor proliferation rate T/C (%) during treatment. (C) Images of orthotopic xenograft nude mice during 28 days of treatment, with each dotted square representing 1 cm in length. (D) Representative images of H&E staining at 20× (Scale bar: 200 μm) and 40× (Scale bar: 50 μm) magnification amplification. Yellow arrows indicate OS necrosis. Data are expressed as the mean ± SEM (n = 6). $^{*}P$ < 0.05, $^{**}P$ < 0.01, and $^{***}P$ < 0.001 *vs* the model group.

in the tumor (Fig. 5B). Although ESRRG expression was notably low in osteosarcoma tissues, a significantly higher concentration of ESRRG proteins was observed in both the nuclei and cytoplasm of osteosarcoma cells following ZYG II treatment. Analysis of Relative IOD revealed that ESRRG expression in IHC more than doubled in the ZYG II treatment group compared to the control group.

3.7. Molecular docking simulates the binding of ZYG II to ESRRG protein

Western blot analysis demonstrated that ZYG II enhances ESRRG protein expression in osteosarcoma. To further elucidate the molecular mechanisms, molecular docking analysis was employed to predict the interaction between ZYG II and ESRRG, comparing it with the interaction between the binding ligand SRC-1 and ESRRG. The results indicated that the affinity score between ZYG II and ESRRG was −7.779 kcal·mol^{-1}, which was higher than that between SRC-1 and ESRRG at −7.67 kcal·mol^{-1}. Hydrogen bonding was identified as the primary factor stabilizing ZYG II to ESRRG (Fig. 4C). The binding positions of ZYG II and SRC-1 in ESRRG showed significant overlap, including GLN426, THR429, LYS430, and GLN433 in both A and B chains, suggesting a highly stable binding between ZYG II and ESRRG protein.

3.8. Knocking down ESRRG weakened the anti-proliferative and G0/G1 arrest effect of ZYG II on SaOS-2, but this effect was not observed in MG-63

Following the transfection of MG-63 and SaOS-2 cells with ESRRG shRNA and subsequent verification of stable ESRRG gene silencing, we subjected negative controls, ESRRG shRNA-transfected cells, and GSK5182 20 μmol·L^{-1}-treated MG-63 and SaOS-2 cells to either ZYG II 15 μmol·L^{-1} treatment or no treatment. EDU staining revealed that negative control, ESRRG shRNA transfection, and GSK5182 20 μmol·L^{-1} treatment did not significantly affect OS cell proliferation (Fig. 6A). In MG-63 cells, proliferation significantly decreased in both ESRRG shRNA-transfected and GSK5182 20 μmol·L^{-1}-treated cells after 24 h of ZYG II 15 μmol·L^{-1} exposure, with the anti-proliferative effect comparable to that observed in the negative control group (Fig. 6B). Conversely, SaOS-2 cells transfected with ESRRG shRNA or treated with GSK5182 at 20 μmol·L^{-1} showed no significant alterations in cell proliferation after 24 h of ZYG II at 15 μmol·L^{-1} exposure.

A consistent pattern was observed regarding alterations in cell cycle distribution (Figs. 7A and 7C). In comparison to negative controls, neither ESRRG shRNA nor GSK5182 treatment at 20 μmol·L^{-1} altered the G_0/G_1 phase cycle distribution of MG-63 and SaOS-2 cells. In MG-63 cells, irrespective of ESRRG knockdown or

inhibition, the proportion of G_0/G_1 phase cells increased following treatment with ZYG II at 15 μmol·L^{-1} for 24 h. However, in SaOS-2 cells, knocking down or inhibiting the ESRRG gene prevented the G_0/G_1 phase arrest that would have occurred with ZYG II treatment.

3.9. Knocking down ESRRG weakened the pro-apoptotic effect of ZYG II on MG-63 and SaOS-2 cells

Consistent with the findings related to cell proliferation and cell cycle progression, the application of ESRRG shRNA or

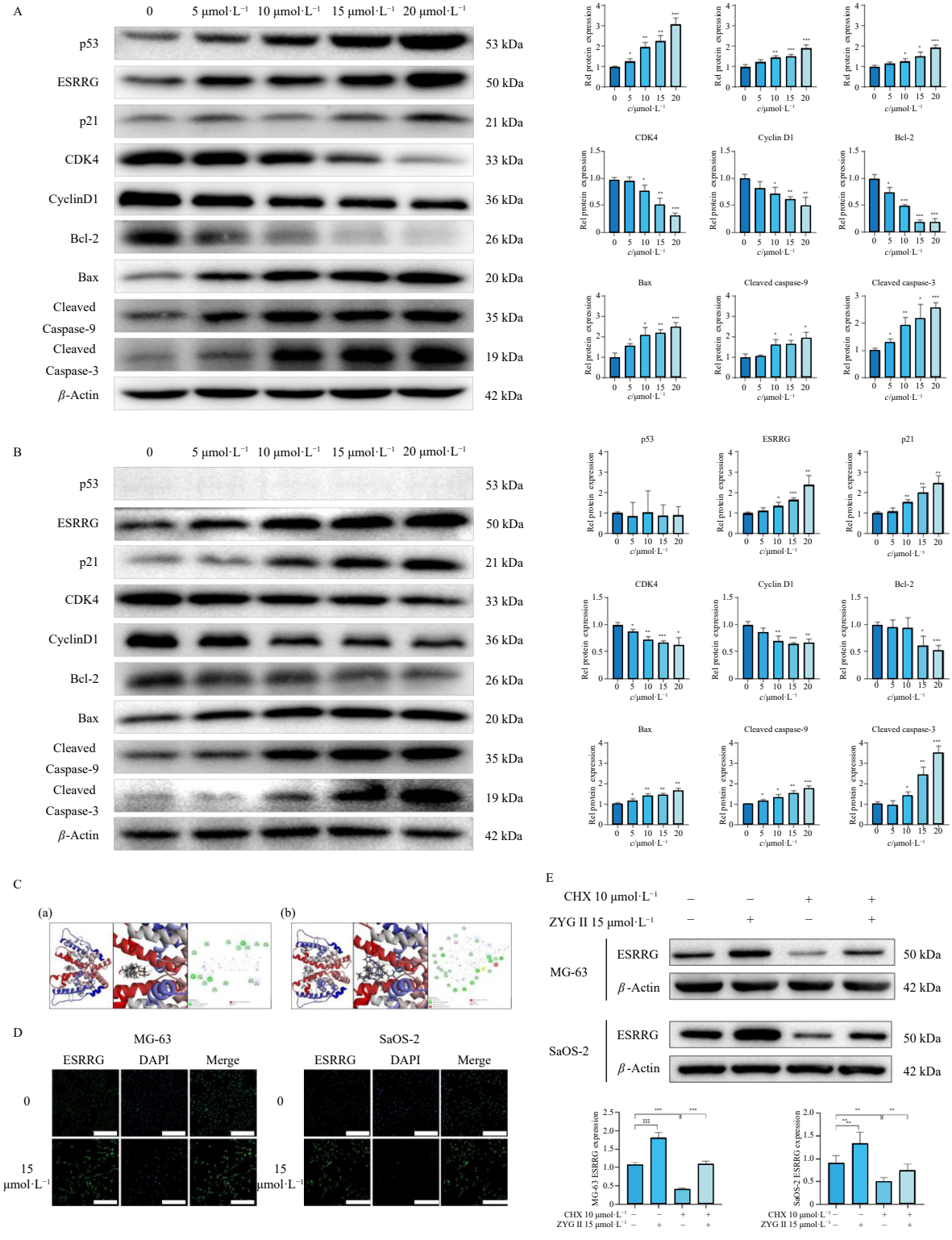

Fig. 4 Effects of ZYG Ⅱ treatment on protein expressions in MG-63 cells and SaOS-2 cells *in vitro*. (A) Western blot analysis of the expression levels of p53, ESSRRG, p21, CDK4, Cyclin D1, Bcl-2, Bax, Cleaved Caspase-9, and Cleaved Caspase-3 in MG-63 cells and SaOS-2 cells treataed with ZYG Ⅱ in a dose-dependent manner. The internal control antibody was *β*-actin. Immunoblot bands (left) and relative protein quantity (right) in MG-63 cells. (B) Immunoblot bands (left) and relative protein quantity (right) in SaOS-2 cells. (C) Binding mode of ZYG Ⅱ and SRC-1 to ESRRG by molecular docking. (a) ZYG Ⅱ docked to ESRRG. (b) SRC-1 docked to ESRRG. Overview of the crystal structures of ZYG Ⅱ and ESRRG (Left); Details of binding pocket interactions (Middle); 2D interactions of compounds and their targets (Right). (D) Immunofluorescence for OS cells, ESRRG is labeled with green fluorescence. Scale bar: 200 μm. (E) CHX treatment was used to inhibit protein synthesis, and the effects of ZYG II on ESRRG protein synthesis and degradation were observed. All data are expressed as mean ± SEM (n = 3). $^{*}P < 0.05$, $^{**}P < 0.01$, and $^{***}P < 0.001$ *vs* Con.

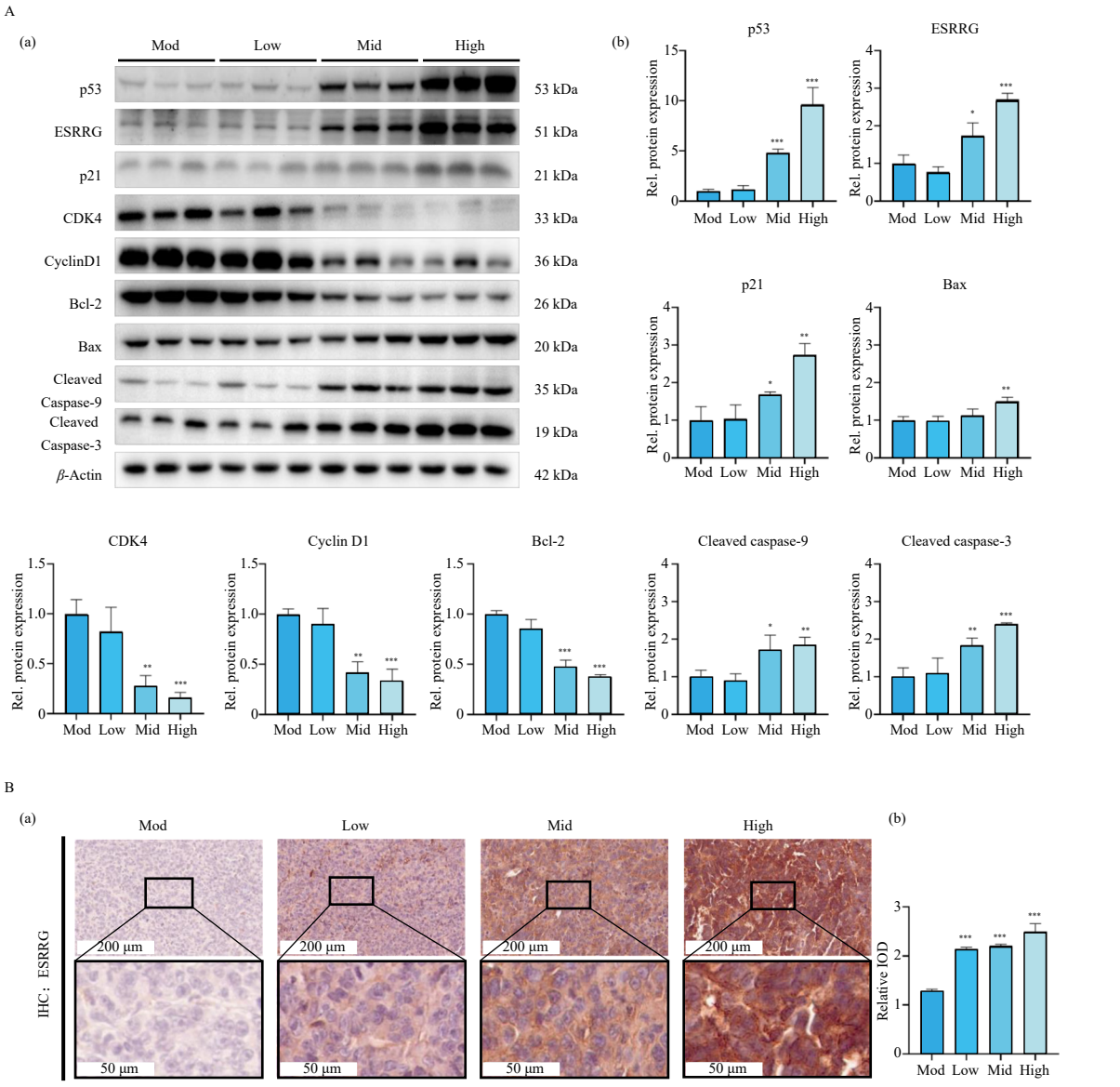

Fig. 5 Effects of ZYG Ⅱ on the expressions of ESRRG, p53 and other proteins in nude mouse model of OS. (A) Western blot analysis of the effects of ZYG Ⅱ on p53, ESRRG, p21, CDK4, Cyclin D1, Bcl-2, Bax, Cleaved Caspase-9, and Cleaved Caspase-3 in a nude mouse model of osteosarcoma. (a) Protein banding results. The internal control antibody was β-Actin. (b) Histogram depicting relative quantities of each protein. (B) Immunohistochemistry of ESRRG expression in OS tissues of nude mice treated with ZYG Ⅱ. (a) Representative images of ESRRG IHC staining at 20× (Scale bar: 200 μm) and 40 × (Scale bar: 50 μm) amplification. Brown coloration indicates ESRRG positivity. (b) Histogram of relative IOD. All data are expressed as mean ± SEM (n = 3). $^{*}P < 0.05$, $^{**}P < 0.01$, and $^{***}P < 0.001$ *vs* the model group.

GSK5182 at 20 μmol·L^{-1} exhibited minimal effects on apoptosis in OS cells (Figs. 7B and 7D). Nevertheless, while the percentage of apoptotic cells in MG-63 and SaOS-2 cells with ESRRG knockdown or inhibition increased significantly following ZYG II treatment, this increase was substantially lower compared to that observed in negative control OS cells treated with ZYG II.

3.10. ESRRG collaboratively activates the p53 downstream signal to block the cell cycle and promote apoptosis

In the MG-63 negative control group, ZYG II treatment demonstrated an increase in p53 expression. Following the inhibition or knockdown of ESRRG, ZYG II therapy maintained its capacity to enhance p53 expression in MG-63, showing no significant difference compared to the negative controls treated with ZYG II (Fig. 8A). In MG-63 and SaOS-2 cells, after ESRRG knockdown or inhibition, no significant difference was observed in the expression levels of p21, CDK4, and CyclinD1 proteins related to the downstream cycle of p53. However, the significant differences in p21, CDK4, and CyclinD1 proteins induced by ZYG II were attenuated (Figs. 8A and 8B).

Following ESRRG knockdown or inhibition, distinct alterations in the expression levels of p53-mediated apoptosis-related proteins, including Bcl-2, Bax, Cleaved Caspase-9, and Cleaved Caspase-3, were observed in OS cells. ZYG II notably suppresses Bcl-2 expression in OS cells. However, this inhibitory effect was significantly mitigated when ESRRG expression was inhibited by GSK5182. While ESRRG does not influence Bax expression in MG-63 cells, it substantially inhibits its expression in SaOS2 cells. ESRRG's impact on Cleaved Caspase-9 was minimal, with only a slight reduction in the elevated protein expression induced by ZYG II treatment after inhibiting MG-63 with GSK5182. In MG-63 cells, reduced ESRRG expression weakened the inducible effect of ZYG II on Cleaved Caspase-3. Concurrently, SaOS-2 cells exhibited significant suppression of Cleaved Caspase-3 expression upon decreased ESRRG expression.

4. Discussion

Ziyuglycoside constitutes the primary component of *S. offi-*

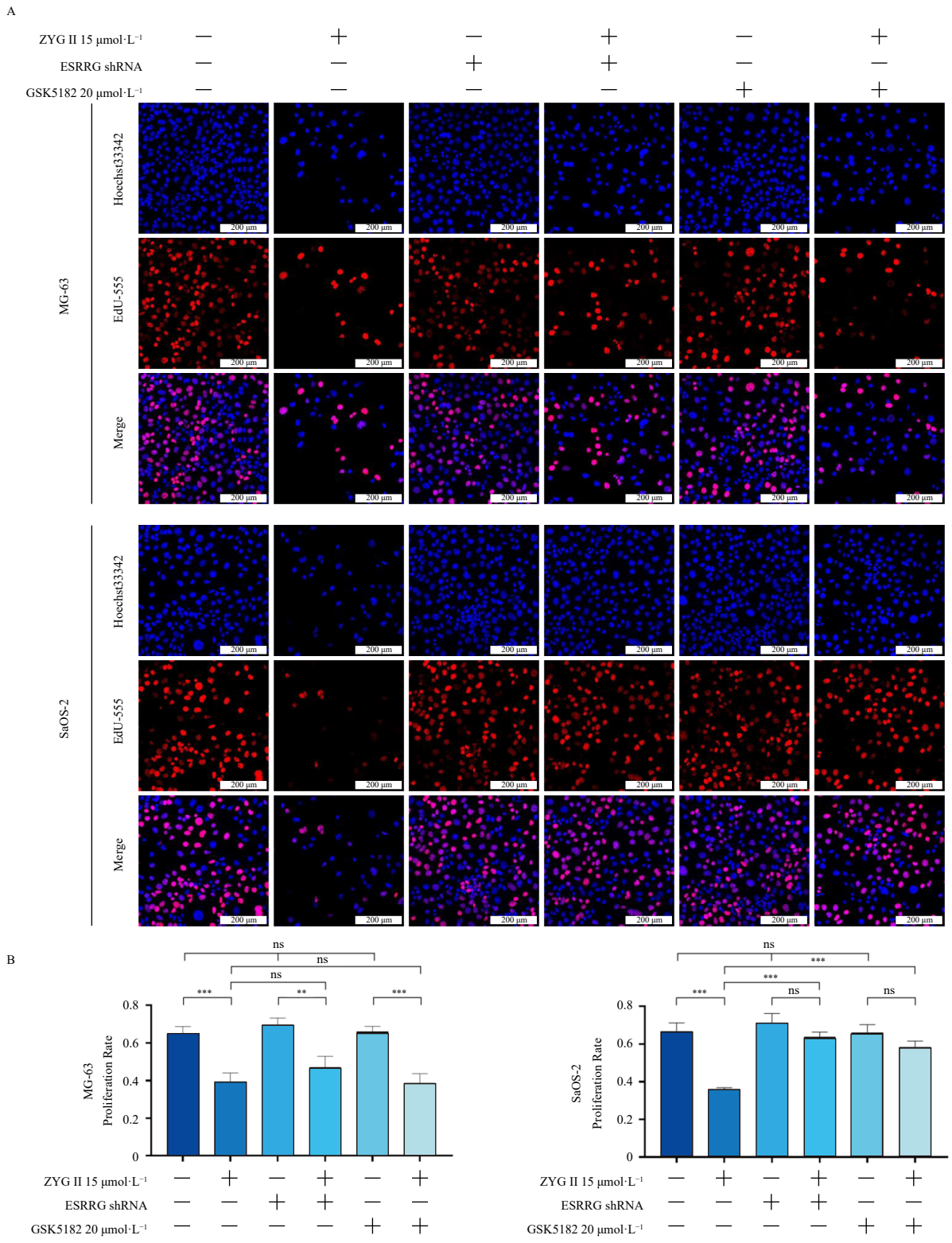

Fig. 6 Effects of ZYGII on the regulation of MG-63 and SaOS-2 cell proliferation was examined through reduction of ESRRG by ESRRG shRNA and GSK5182. (A) Cell proliferation rate was detected by EdU staining. Red staining indicates proliferation (EdU +), while blue staining marks the nucleus. Scale bar: 200 μm. (B) EdU incorporation was calculated as the ratio of EdU+ cells/total cells, quantified by ImageJ. All data are expressed as mean ± SEM (n = 3). $^{*}P < 0.05$, $^{**}P < 0.01$, and $^{***}P < 0.001$.

cinalis, consisting of ZYG I and ZYG II, with the latter functioning as the principal metabolite of the former [37]. ZYG II belongs to the triterpenoid class of compounds, many of which have demonstrated broad-spectrum anti-tumor effects, including oleanane, ursane, lupane, dammarane, cholestane, spirostane, furostane and cardenolides [38]. ZYG II also exhibits various anti-tumor properties, as confirmed by *in vitro* experiments that showed its reduced cytotoxic activity towards normal cells compared to malignant cells, indicating its potential significance in drug development [16-23]. However, the anticancer capabilities of this compound against osteosarcoma remained unclear. This study reveals, for the first time, that ZYG II demonstrates anti-cancer effects on osteosarcoma through the inhibition of proliferation, cell cycle arrest, and induction of apoptosis.

The CCK8 assay confirmed that ZYG II exhibits an inhibitory effect on various OS cells, with an IC_{50} ranging between 15 and 21

μmol·L^{-1} (Fig. 1A). This finding informed the selection of ZYG II concentrations at 5, 10, 15, and 20 μmol·L^{-1} for subsequent *in vitro* experiments. EdU detection further revealed that the proliferation capacity of osteosarcoma cells decreased with increasing dosages of ZYG II (Figs. 1 and S1 B&C). To elucidate the efficacy of ZGY II more comprehensively, an orthotopic xenograft osteosarcoma model was established and treated with varying doses of ZGY II (Fig. 3 A). The antitumor activity of ZYG II was assessed by measuring the relative tumor volume and relative tumor proliferation rate. Results indicated that ZYG II doses exceeding 20 mg·kg^{-1} significantly suppressed osteosarcoma growth (Fig. 3B). While the anti-osteosarcoma effect of ZYG II *in vivo* at low and

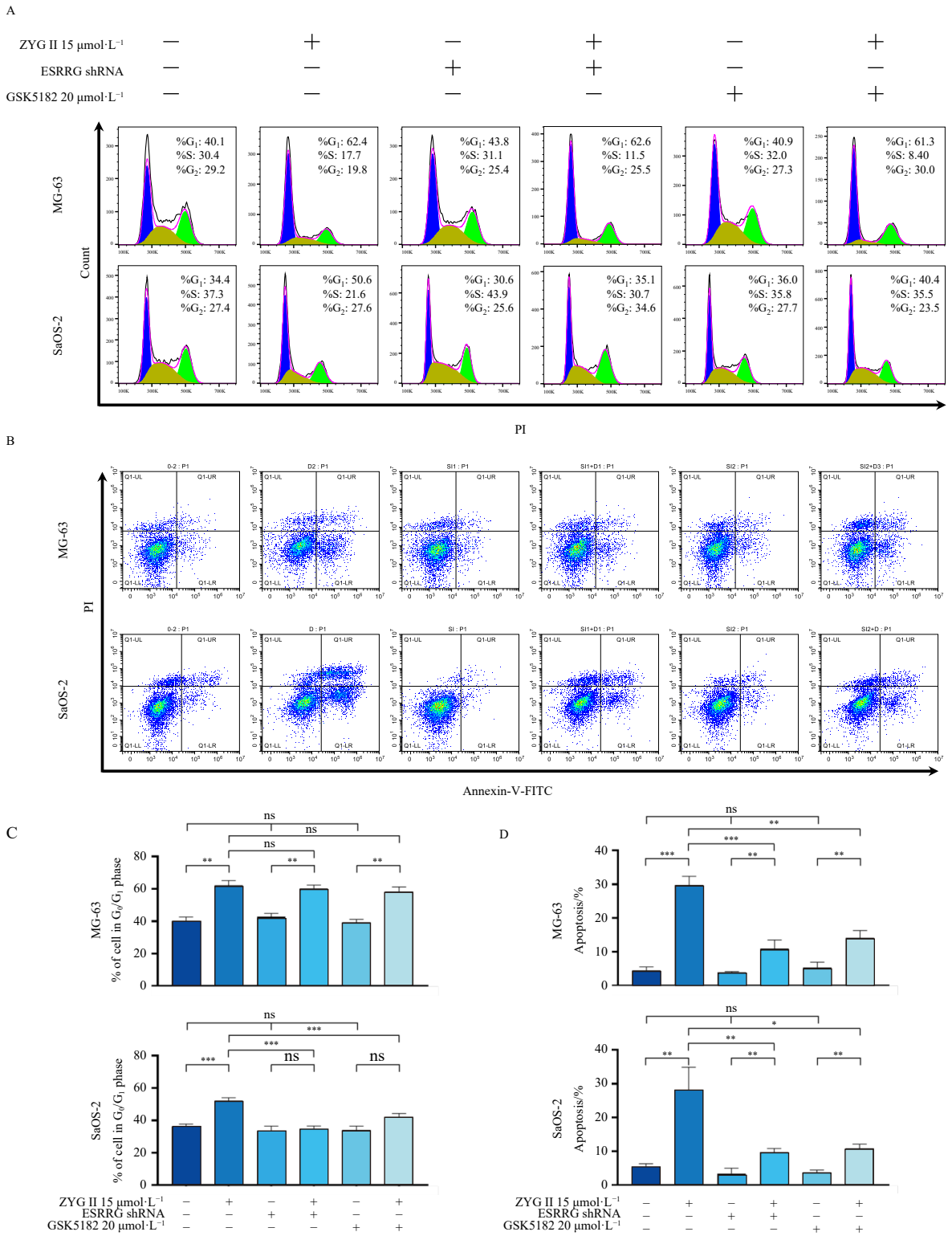

Fig. 7 The impact of ZYG II on the regulation of MG-63 and SaOS-2 cell cycle and apoptosis was examined through ESRRG reduction. ESRRG-reduced MG-63 and SaOS-2 cells were generated by ESRRG shRNA or 20 μmol·L^{-1} GSK5182 treatment. (A, C) Effect of ZYGII administration on cell cycle distribution of MG-63 and SaOS-2 with or without ESRRG knockdown. (B, D) Effect of ZYGII administration on apoptosis of MG-63 and SaOS-2 with or without ESRRG knockdown. Live cells were represented by Annexin V−/PI−, apoptosis cells were represented by Annexin V+/PI−, Late apoptotic and necrotic cells were represented by Annexin V+/PI+, and schistocytes generated by mechanical damage were represented by PI+/Annexin+. All data are expressed as mean ± SEM (n = 3). $^{*}P < 0.05$, $^{**}P < 0.01$, and $^{***}P < 0.001$.

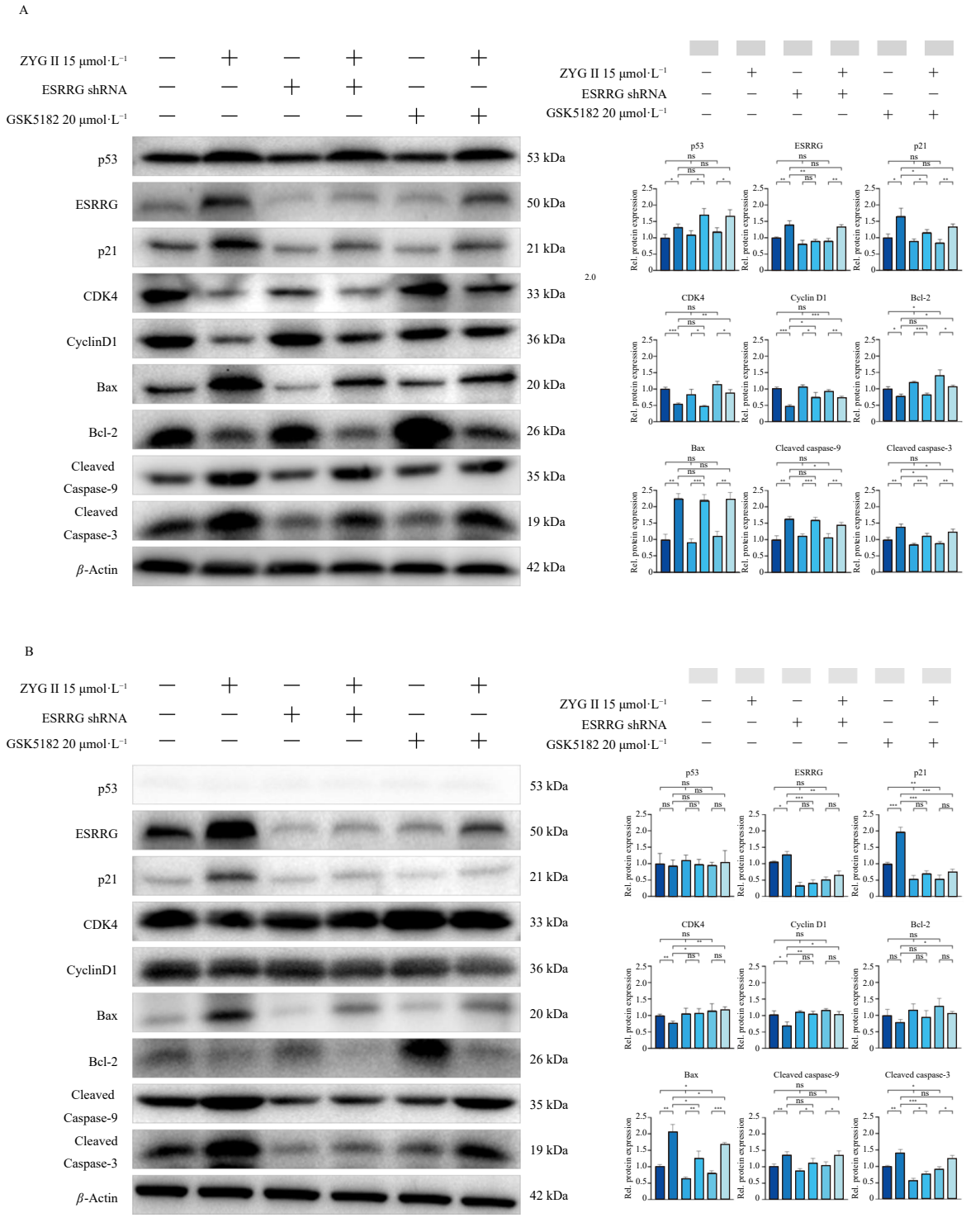

Fig. 8 Effects of ZYG II on the regulation of MG-63 and SaOS-2 cells protein expression was examined through reduction of ESRRG. ESRRG-reduced MG-63 and SaOS-2 cells were constructed by ESRRG shRNA or 20 μmol·L^{-1} GSK5182 treatment. The protein expression levels of p53, ESSRRG, p21, CDK4, Cyclin D1, Bcl-2, Bax, Cleaved Caspase-9, and Cleaved Caspase-3 in 15 μmol·L^{-1} ZYG II-treated normal cells and ESRRG-reduced OS cells were compared. β-actin served as the internal control antibody. (A) Immunoblot bands (left) and relative protein quantity (right) on MG-63 cells with or without ESRRG inhibition. (B) Immunoblot bands (left) and relative protein quantities (right) on SaOS-2 cells with or without ESRRG inhibition. All data are expressed as mean ± SEM (n = 3). $^{*}P < 0.05$, $^{**}P < 0.01$, and $^{***}P < 0.001$.

medium doses was not significant, high-dose administration may present potential drug off-target and safety risks. However, previous studies have demonstrated that ZYG II exhibits lower toxicity to normal liver and kidney cells compared to malignant cells [19]. Consistently, recent research involving ZYG II administration in mice reported no drug-induced damage, with the highest dose administered being 18 mg·kg^{-1} [23]. Liver HE staining and serum AST and ALT detection indicated limited liver damage at this dose. Further investigation into potential drug safety and off-target effects through the construction of targeted drug vectors would be informative [39,40].

Previous studies have demonstrated that ZYG II possesses the ability to induce cell cycle arrest and apoptosis in various tumors [17,21,41]. This investigation employed flow cytometry to evaluate the cell cycle distribution and apoptotic cell ratio of OS cells following ZYG II treatment (Figs. 2 and S2). The findings indicate that ZYG II can arrest osteosarcoma cells at the G_0/G_1 phase while simultaneously inducing apoptosis. Further analysis revealed that

ZYG II modulates the expression of p53 and its downstream signals, evidenced by increased levels of p53, p21, Bax, Cleaved Caspase-9, and Cleaved Caspase-3 proteins, alongside decreased expression of CDK4, Cyclin D1, and Bcl-2 proteins (Fig. 4). These results align with ZYG II's observed effects on G_0/G_1 phase arrest and apoptosis induction in osteosarcoma cells.

The tumor suppressor p53 plays a crucial role in inhibiting osteosarcoma development through cell cycle arrest and apoptosis [11]. The translation of p53 activates the transcription of p21WAF1/CIP1, resulting in the p21 protein inhibiting CDK4 and Cyclin D1 expression, which prevents cells from transitioning from G_0 phase to S_1 phase [11, 42, 43]. The p53 signal promotes apoptosis through various pathways, with a critical step being the direct activation of Bax by p53 and the inhibition of Bcl-2, which has a suppressive effect on activated Bax [43, 44]. Activated Bax, in turn, promotes the activation of Caspase9 and Caspase3 through the apoptosome, initiating and executing the process of cell apoptosis [45]. Collectively, these findings suggest that ZYG II inhibits osteosarcoma development by inducing cell cycle arrest and promoting apoptosis through the activation of the p53 signaling pathway.

This study revealed that ZYG II could regulate the cell cycle and apoptosis of both p53-positive MG-63 cells and p53-negative SaOS-2 cells. This finding suggests that ZYG II's regulation of osteosarcoma proliferation, cell cycle, and apoptosis is not solely dependent on p53, but also influenced by other factors. Cell proliferation and cell cycle could be regulated without p53 interference by controlling external signals such as growth factors or directly modulating downstream signals of p53, including p16, p21, and p27. Similarly, cell apoptosis could be promoted independently of p53 by activating p53-independent apoptosis pathways or directly modulating downstream signals of p53-induced apoptosis.

ESRRG comprises a set of transcription factors that modulate gene expression in response to diverse stimuli, including hormones, lipids, and small molecules. It has been demonstrated to function as a tumor suppressor, playing a role in the occurrence and development of various tumors [28, 29, 46]. Previous studies have revealed that ESRRG is highly concentrated at the CDKN1A gene, which encodes the p21 protein. Conversely, its depletion results in decreased CDKN1A RNA expression [30]. In prostate and liver cancers, ESRRG can regulate the p21 and p27 genes through direct transactivation of their promoters, with its effect highly dependent on the cellular environment [27-29]. In this study, the administration of ZYG II led to an upregulation of ESRRG protein expression in osteosarcoma, both *in vivo* and *in vitro*. Furthermore, a comparison of ESRRG protein expression with CHX treatment indicated that ZYG II could mitigate the negative influence of the protein synthesis pathway on ESRRG. Molecular docking prediction results revealed that ZYG II and SRC-1 had multiple overlapping binding positions in ESRRG, with ZYG II demonstrating stronger affinity. This suggests that ZYG II may form a highly stable interaction with ESRRG.

To further elucidate the role of ESRRG in ZYG II-mediated inhibition of osteosarcoma, particularly in relation to p53, this study established stable MG-63 and SaOS-2 cell lines with reduced ESRRG expression using ESRRG shRNA and GSK5182, an inverse agonist of ESRRG. The research revealed that the antiproliferative and cell cycle arrest effects of ZYG II on MG-63 cells with diminished ESRRG expression were comparable to those observed in MG-63 cells with normal ESRRG expression (Fig. 6). However, in SaOS-2 cells with ESRRG knockdown, the anti-proliferative and cell cycle-arresting effects of ZYG II were significantly attenuated (Figs. 6&7). In the presence of p53, ZYG II's regulation of osteosarcoma cell proliferation and the cell cycle was independent of ESRRG expression. Only in the absence of p53 did the upregulation of ESRRG by ZYG II manifest its effects on proliferation and cell cycle regulation. Furthermore, the pro-apoptotic effect of ZYG II was reduced in both MG-63 and SaOS-2 cells with decreased ESRRG expression (Fig. 7), suggesting that ZYG II could upregulate ESRRG to exert its pro-apoptotic role regardless of p53 expression. Silencing ESRRG did not affect p53 expression in MG-63 cells, with or without ZYG II treatment (Fig. 8A). Consistently, ESRRG protein expression was observed and upregulated after ZYG II administration in both p53-positive MG-63 cells and p53-negative SaOS-2 cells (Fig. 8). This indicates the absence of mutual regulation between p53 and ESRRG during ZYG II treatment of osteosarcoma. Independent upregulation of either p53 or ESRRG can inhibit cell proliferation, arrest the cell cycle, and promote apoptosis. However, only when both p53 and ESRRG are simultaneously absent are the inhibitory effects of ZYG II on osteosarcoma cell proliferation, cell cycle arrest, and apoptosis promotion significantly diminished.

This study further elucidates the molecular regulatory mechanism by which ESRRG influences osteosarcoma progression through cell cycle regulation and apoptosis induction. In p53-positive MG-63 cells, reducing ESRRG does not significantly impact the regulation by ZYG II of downstream molecules related to the p53 signaling pathway. Conversely, in p53-negative SaOS-2 cells, reducing ESRRG expression significantly alters the regulatory effects of ZYG II on the protein expression of p21, CDK4, Cyclin D1, Bax, and Cleaved Caspase3 in osteosarcoma cells. During the treatment of OS using ZYG II therapy, ESRRG appears to regulate downstream signaling pathways of p53, but only in the absence of p53. In summary, ZYG II upregulates the expression of p53 and ESRRG, which regulates the downstream p21/CDK4/cyclin D1 pathway, leading to cell cycle arrest at the G0/G1 phase. Additionally, it modulates the Bax/Bcl-2 ratio, activates Caspase-9 and Caspase-3, and promotes cell apoptosis, thereby inhibiting the progression of osteosarcoma.

5. Conclusion

This study demonstrates that ZYG II effectively inhibits osteosarcoma both *in vitro* and *in vivo*. Through the utilization of ESRRG shRNA and the ESRRG inverse agonist GSK5182 to suppress ESRRG expression, the research elucidates that ZYG II inhibits osteosarcoma progression via coordinated regulation between p53 and ESRRG, leading to cell cycle arrest and enhanced apoptosis.

Funding

This work was supported by the National Key Research and Development Program of China (No. 2022YFC3502100), the National Natural Science Foundation of China (No. 82274197), the Cutting Edge Development Fund of Advanced Medical Research InstituteMunicipal Science and (No. GYY2023QY01), and the Technology Project of Jinan City (No. 202228099).

Supporting Information

Supporting information for this study is available upon request via email to the corresponding authors.

Declaration of competing interest

These authors have no conflict of interest to declare.

References

1 Siegel RL, Miller KD, Wagle NS, et al. Cancer statistics, 2023. *CA Cancer J Clin*. 2023;73(1):17-48. https://doi.org/10.3322/caac.21763.
2 Strauss SJ, Frezza AM, Abecassis N, et al. Bone sarcomas: ESMO-EURACAN-GENTURIS-ERN PaedCan Clinical Practice Guideline for diagnosis, treatment and follow-up. *Ann Oncol*. 2021;32(12):1520-1536. https://doi.org/10.1016

/j.annonc.2021.08.1995.
3 Pin F, Prideaux M, Bonewald LF, et al. Osteocytes and cancer. *Curr Osteoporos Rep*. 2021;19(6):616-625. https://doi.org/10.1007/s11914-021-00712-9.
4 Cole S, Gianferante DM, Zhu B, et al. Osteosarcoma: a surveillance, epidemiology, and end results program-based analysis from 1975 to 2017. *Cancer-Am Cancer Soc*. 2022;128(11):2107-2118.
5 Zhao X, Wu Q, Gong X, et al. Osteosarcoma: a review of current and future therapeutic approaches. *Biomed Eng Online*. 2021;20(1):24. https://doi.org/10.1186/s12938-021-00860-0.
6 Da W, Tao Z, Meng Y, et al. A 10-year bibliometric analysis of osteosarcoma and cure from 2010 to 2019. *BMC Cancer*. 2021;21(1):115. https://doi.org/10.1186/s12885-021-07818-4.
7 Beird HC, Bielack SS, Flanagan AM, et al. Osteosarcoma. *Nat Rev Dis Primers*. 2022;8(1):77. https://doi.org/10.1038/s41572-022-00409-y.
8 Gerstung M, Jolly C, Leshchiner I, et al. The evolutionary history of 2, 658 cancers. *Nature*. 2020;578(7793):122-128. https://doi.org/10.1038/s41586-019-1907-7.
9 Tobeiha M, Rajabi A, Raisi A, et al. Potential of natural products in osteosarcoma treatment: focus on molecular mechanisms. *Biomed Pharmacother*. 2021;144:112257. https://doi.org/10.1016/j.biopha.2021.112257.
10 Kazantseva L, Becerra J, Santos-Ruiz L. Traditional medicinal plants as a source of inspiration for osteosarcoma therapy. *Molecules*. 2022;27(15):5008. https://doi.org/10.3390/molecules27155008.
11 Engeland K. Cell cycle regulation: p53-p21-RB signaling. *Cell Death Differ*. 2022;29(5):946-960. https://doi.org/10.1038/s41418-022-00988-z.
12 Sanchez-Rivera FJ, Ryan J, Soto-Feliciano YM, *et al*. Mitochondrial apoptotic priming is a key determinant of cell fate upon p53 restoration. *P Natl Acad Sci USA*. 2021;118(23):e2019740118. https://doi.org/10.1073/pnas.2019740118.
13 Zhou P, Li J, Chen Q, et al. A comprehensive review of genus *Sanguisorba*: traditional uses, chemical constituents and medical applications. *Front Pharmacol*. 2021;12:750165. https://doi.org/10.3389/fphar.2021.750165.
14 Motoc ACT, Kokeric T, Tripon S, et al. *Sanguisorba minor* Scop.: an overview of its phytochemistry and biological effects. *Plants-Basel*. 2023;12(11):2128. https://doi.org/10.3390/plants12112128.
15 Jang E, Inn KS, Jang YP, et al. Phytotherapeutic activities of *Sanguisorba officinalis* and its chemical constituents: a review. *Am J Chin Med*. 2018;46(2):299-318. https://doi.org/10.1142/S0192415X18500155.
16 Zhong Y, Li XY, Zhou F, et al. Ziyuglycoside II inhibits the growth of digestive system cancer cells through multiple mechanisms. *Chin J Nat Med*. 2021;19(5):351-363. https://doi.org/10.1016/S1875-5364(21)60033-X.
17 Zhu AK, Zhou H, Xia JZ, et al. Ziyuglycoside II-induced apoptosis in human gastric carcinoma BGC-823 cells by regulating Bax/Bcl-2 expression and activating caspase-3 pathway. *Braz J Med Biol Res*. 2013;46(8):670-675. https://doi.org/10.1590/1414-431X20133050.
18 Lkhagvasuren K, Kim JK. Ziyuglycoside II induces caspases-dependent and caspases-independent apoptosis in human colon cancer cells. *Toxicol In Vitro*. 2019;59:255-262. https://doi.org/10.1016/j.tiv.2019.04.028.
19 Liao W, Fan L, Zheng Z, et al. Ziyuglycoside II exerts antiproliferative and antimetastasis effects on hepatocellular carcinoma cells. *Anticancer Drugs*. 2020;31(8):819-827. https://doi.org/10.1097/CAD.0000000000000918.
20 Zhu X, Wang K, Zhang K, et al. Ziyuglycoside II inhibits the growth of human breast carcinoma MDA-MB-435 cells *via* cell cycle arrest and induction of apoptosis through the mitochondria dependent pathway. *Int J Mol Sci*. 2013;14(9):18041-18055. https://doi.org/10.3390/ijms140918041.
21 Zhu X, Wang K, Zhang K, et al. Ziyuglycoside II induces cell cycle arrest and apoptosis through activation of ROS/JNK pathway in human breast cancer cells. *Toxicol Lett*. 2014;227(1):65-73. https://doi.org/10.1016/j.toxlet.2014.03.015.
22 Wang K, Zou P, Zhu X, et al. Ziyuglycoside II suppresses the aggressive phenotype of triple negative breast cancer cells through regulating Src/EGFR-dependent ITGB4/FAK signaling. *Toxicol In Vitro*. 2019;61:104653. https://doi.org/10.1016/j.tiv.2019.104653.
23 Fang H, Xie X, Liu P, et al. Ziyuglycoside II alleviates cyclophosphamide-induced leukopenia in mice *via* regulation of HSPC proliferation and differentiation. *Biomed Pharmacother*. 2020;132:110862. https://doi.org/10.1016/j.biopha.2020.110862.
24 Chen X, Li B, Gao Y, et al. Saponins from *Sanguisorba officinalis* improve hematopoiesis by promoting survival through FAK and Erk1/2 activation and modulating cytokine production in bone marrow. *Front Pharmacol*. 2017;8:130. https://doi.org/10.3389/fphar.2017.00130.
25 Nam SH, Lkhagvasuren K, Seo HW, et al. Antiangiogenic effects of ziyuglycoside II, a major active compound of *Sanguisorba officinalis* L.. *Phytother Res*. 2017;31(9):1449-1456. https://doi.org/10.1002/ptr.5874.
26 Nakadai T, Shimada M, Ito K, et al. Two target gene activation pathways for orphan ERR nuclear receptors. *Cell Res*. 2023;33(2):165-183. https://doi.org/10.1038/s41422-022-00774-z.
27 Kim JH, Choi YK, Byun JK, et al. Estrogen-related receptor gamma is upregulated in liver cancer and its inhibition suppresses liver cancer cell proliferation *via* induction of p21 and p27. *Exp Mol Med*. 2016;48(3):e213. https://doi.org/10.1038/emm.2015.115.
28 Yu S, Wang X, Ng CF, et al. ERRgamma suppresses cell proliferation and tumor growth of androgen-sensitive and androgen-insensitive prostate cancer cells and its implication as a therapeutic target for prostate cancer. *Cancer Res*. 2007;67(10):4904-4914. https://doi.org/10.1158/0008-5472.CAN-06-3855.
29 Kang MH, Choi H, Oshima M, et al. Estrogen-related receptor gamma functions as a tumor suppressor in gastric cancer. *Nat Commun*. 2018;9(1):1920. https://doi.org/10.1038/s41467-018-04244-2.
30 Field MG, Kuznetsoff JN, Zhang MG, et al. RB1 loss triggers dependence on ESRRG in retinoblastoma. *Sci Adv*. 2022;8(33):eabm8466. https://doi.org/10.1126/sciadv.abm8466.
31 Eichner LJ, Perry MC, Dufour CR, et al. miR-378* mediates metabolic shift in breast cancer cells *via* the PGC-1β/ERRγ transcriptional pathway. *Cell Metab*. 2010;12(4):352-361. https://doi.org/10.1016/j.cmet.2010.09.002.
32 Su N, Qiu H, Chen Y, et al. miR-205 promotes tumor proliferation and invasion through targeting ESRRG in endometrial carcinoma. *Oncol Rep*. 2013;29(6):2297-2302. https://doi.org/10.3892/or.2013.2400.
33 Zirngibl RA, Chan JS, Aubin JE. Divergent regulation of the Osteopontin promoter by the estrogen receptor-related receptors is isoform- and cell context dependent. *J Cell Biochem*. 2013;114(10):2356-2362. https://doi.org/10.1002/jcb.24583.
34 Cardelli M, Auin JE. ERRγ is not required for skeletal development but is a RUNX2-dependent negative regulator of postnatal bone formation in male mice. *PLoS One*. 2014;9(10):e109592. https://doi.org/10.1371/journal.pone.0109592.
35 Kim HJ, Yoon HJ, Lee DK, et al. The estrogen-related receptor gamma modulator, GSK5182, inhibits osteoclast differentiation and accelerates osteoclast apoptosis. *BMB Rep*. 2021;54(5):266-271. https://doi.org/10.5483/BMBRep.2021.54.5.243.
36 Higuchi T, Sugisawa N, Miyake K, et al. The combination of olaratumab with doxorubicin and cisplatinum regresses a chemotherapy-resistant osteosarcoma in a patient-derived orthotopic xenograft mouse model. *Transl Oncol*. 2019;12(9):1257-1263. https://doi.org/10.1016/j.tranon.2019.06.002.
37 Li ZF, Zhou MY, Tan T, et al. A sample and sensitive HPLC-MS/MS method for simultaneous determination of ziyuglycoside I and its metabolite ziyuglycoside II in rat pharmacokinetics. *Molecules*. 2018;23(3):543. https://doi.org/10.3390/molecules23030543.
38 Elekofehinti OO, Iwaloye O, Olawale F, et al. Saponins in cancer treatment: current progress and future prospects. *Pathophysiology*. 2021;28(2):250-272. https://doi.org/10.3390/pathophysiology28020017.
39 Lan HR, Zhang YN, Han YJ, et al. Multifunctional nanocarriers for targeted drug delivery and diagnostic applications of lymph nodes metastasis: a review of recent trends and future perspectives. *J Nanobiotechnol*. 2023;21(1):247. https://doi.org/10.1186/s12951-023-01990-4.
40 Lu KH, Lu PW, Lin CW, et al. Curcumin in human osteosarcoma: from analogs to carriers. *Drug Discov Today*. 2023;28(2):103437. https://doi.org/10.1016/j.drudis.2022.103437.
41 Bai C, Zhang Z, Zhou L, et al. Repurposing ziyuglycoside II against colorectal cancer *via* orchestrating apoptosis and autophagy. *Front Pharmacol*. 2020;11:576547. https://doi.org/10.3389/fphar.2020.576547.
42 Borrero LJH, El-Deiry WS. Tumor suppressor p53: biology, signaling pathways, and therapeutic targeting. *Biochim Biophys Acta Rev Cancer*. 2021;1876(1):188556. https://doi.org/10.1016/j.bbcan.2021.188556.
43 Boutelle AM, Attardi LD. p53 And tumor suppression: it takes a network. *Trends Cell Biol*. 2021;31(4):298-310. https://doi.org/10.1016/j.tcb.2020.12.011.
44 Vaddavalli PL, Schumacher B. The p53 network: cellular and systemic DNA damage responses in cancer and aging. *Trends Genet*. 2022;38(6):598-612. https://doi.org/10.1016/j.tig.2022.02.010.
45 Hafezi S, Rahmani M. Targeting BCL-2 in cancer: advances, challenges, and perspectives. *Cancers (Basel)*. 2021;13(6):1292. https://doi.org/10.3390/cancers13061292.
46 Guo X, Yue L, Li M, et al. Nuclear receptor estrogen-related receptor gamma suppresses colorectal cancer aggressiveness by regulating Wnt/β-catenin signaling. *Carcinogenesis*. 2022;43(9):865-873. https://doi.org/10.1093/carcin/bgac054.